Article:
Wills, K.A., Tadhunter, C., Holt, J. et al. (2008) Diverse young stellar populations in the intermediate-redshift radio galaxies 3C 213.1 and 3C 459: implications for the evolution of the host galaxies. Monthly Notices of the Royal Astronomical Society, 385 (1). pp. 136-146. ISSN: 0035-8711

https://doi.org/10.1111/j.1365-2966.2008.12865.x

Mon. Not. R. Astron. Soc. **385,** 136–146 (2008) doi:10.1111/j.1365-2966.2008.12865.x

Diverse young stellar populations in the intermediate-redshift radio galaxies 3C 213.1 and 3C 459: implications for the evolution of the host galaxies

K. A. Wills,[1] C. Tadhunter,[1⋆] J. Holt,[1] R. González Delgado,[2] K. J. Inskip,[1] J. Rodríguez Zaurín[1] and R. Morganti[3]

[1]*Department of Physics and Astronomy, University of Sheffield, Sheffield S3 7RH*
[2]*Instituto de Astrofísica de Andalucía, Apdto. 3004, 18080 Granada, Spain*
[3]*ASTRON, PO Box 2, 7990 AA Dwingeloo, the Netherlands*

Accepted 2007 December 14. Received 2007 December 6; in original form 2007 September 19

ABSTRACT

We present European Southern Observatory Very Large Telescope (ESO VLT) and William Herschel Telescope (WHT) spectroscopic observations of two powerful radio galaxies at intermediate redshifts (3C 213.1 and 3C 459), obtained with the aim of establishing the nature and evolutionary status of the host galaxies. Spectral synthesis modelling has been used to demonstrate that young stellar populations (YSP) make a major contribution to the integrated optical light in both sources, contributing at least 37 and 80 per cent of the integrated *B*-band light in 3C 213.1 and 3C 459, respectively. While in the case of 3C 213.1 the YSP has an intermediate age (0.4–0.8 Gyr) and comprises 3–30 per cent of the total stellar mass, adequate fits to the spectra of 3C 459 require a combination of younger (<0.1 Gyr) and intermediate (0.2–1.2 Gyr) age YSP components that together comprise 5–100 per cent of the total stellar mass. Both the optical and far-IR properties of 3C 459 are consistent with its status as an ultraluminous infrared galaxy (ULIRG), and a scenario in which the observed radio source has been triggered close to the peak of star formation activity in a major gas-rich merger. On the other hand, in 3C 213.1 it is likely that the radio source has been triggered (or re-triggered) a significant period *after* the starburst peak, and the far-IR luminosity of the source is substantially lower. Following correction for the contributions of the YSP, the absolute magnitudes of the host galaxies of both sources are relatively modest ($\leqslant 2L_*$), thus demonstrating that powerful radio activity is not always associated with the most massive and luminous elliptical galaxies. These results serve to emphasize that the radio source population is diverse, in terms of both the host galaxy properties and the triggering mechanism(s) for the radio source activity.

Key words: galaxies: active – galaxies: individual: 3C 459 – galaxies: individual: 3C 213.1.

1 INTRODUCTION

Powerful radio galaxies are typically associated with early-type hosts and, as such, studies of these sources provide vital clues to our understanding of both the evolution of early-type galaxies and the triggering of the nuclear activity. Previous work, such as the study presented by Heckman et al. (1986), suggests that for many radio galaxies the accretion of gas during galaxy mergers and interactions can trigger the activity, as evidenced by the presence of distinct optical morphologies including arcs, tails and bridges. In hierarchical galaxy evolution models, mergers can both fuel the active galactic nuclei (AGN) activity and, in many cases, also trigger a starburst (Mihos & Hernquist 1996; Kauffmann & Haehnelt 2000; di Matteo, Springel & Hernquist 2005). Indeed, young stellar populations (YSP) have now been identified spectroscopically in ∼20–30 per cent of radio galaxies (see Aretxaga et al. 2001; Tadhunter et al. 2002; Wills et al. 2002, 2004; Raimann et al. 2005). The identification of a starburst, and, in particular, the determination of the age of the YSP, provides a useful tool for establishing the time-scales of activity within a radio galaxy relative to the triggering merger event. Furthermore, the determination of the YSP contribution to the total luminosity of the galaxy has important consequences for our understanding of the stellar content of radio galaxy hosts, with potential

⋆E-mail: c.tadhunter@sheffield.ac.uk

implications for the long-accepted model that the elliptical galaxy hosts are dominated by a bulge of relatively old stellar populations (OSP; e.g. McLure et al. 1999).

In order to fully exploit the stellar populations as probes of the triggering of the activity and the evolution of the host galaxies, we are undertaking a programme of detailed spectroscopy and continuum modelling of a sample of radio galaxies that show clear evidence of YSP in their optical spectra. Results for a subset of this sample have been published in Tadhunter et al. (2005) and Holt et al. (2006, 2007), while the implications of results for the sample as a whole will be discussed in a forthcoming paper (Tadhunter et al., in preparation). In this article, we concentrate on the final two intermediate-redshift ($z \sim 0.2$) radio galaxies from our sample – 3C 459 and 3C 213.1 – for which our previous spectroscopic data (Tadhunter et al. 2002; Holt 2005) indicate a particularly large proportional contribution from YSP at optical wavelengths, thus allowing more detailed modelling of their YSP than is possible for most radio galaxies.

3C 459 is identified with a 17.55 *V* magnitude N-galaxy at a redshift of 0.2199 (Spinrad et al. 1985; Eracleous & Halpern 1994) and is classified as a narrow-line radio galaxy (Tadhunter et al. 1993), albeit with relatively low emission line equivalent widths and evidence for strongly blueshifted components (Holt 2005). It was first noted as unusual during a spectroscopic study of a sample of galaxies by Miller (1981) who found that, unusually for a radio galaxy, its spectrum shows higher order Balmer lines in absorption. On this basis, it was tentatively identified as an elliptical with recent star formation (see also Tadhunter et al. 2002). Another interesting feature of this source is that, based on *IRAS* observations, its far-IR luminosity is unusually high for a radio galaxy ($L_{\rm IR} = 1.6 \times 10^{12}\,{\rm L}_{\odot}$) – approximately 10 times brighter than most other radio sources from the 2 Jy sample at comparable redshifts (see Tadhunter et al. 2002, 2007). This leads to its classification as an ultraluminous infrared galaxy (ULIRG; see Sanders & Mirabel 1996 for definition). In common with many ULIRGs, the host galaxy of 3C 459 is not a normal, quiescent elliptical galaxy, but instead exhibits a fan-like protrusion suggestive of a recent tidal encounter (Heckman et al. 1986). In the radio, 3C 459 is also unusual in the sense that it shows a highly asymmetric double-lobed Fanaroff–Riley type II (FRII) radio structure of diameter 8.5 arcsec (27 kpc), as well as a strong steep spectrum core (e.g. Thomasson, Saikia & Muxlow 2003).

3C 213.1 is identified with a 19.0 *V* magnitude galaxy (Wyndham 1966) at a redshift of $z = 0.194$ (Smith & Spinrad 1980). It is found to be located close to the edge of a small group of galaxies of which it is one of the brightest members (Wyndham 1966). Optical spectra of this source reveal it to be a narrow-line radio galaxy of relatively modest emission line luminosity, with evidence for blueshifted emission line components, as well as the detection of strong Balmer absorption lines (Gelderman & Whittle 1994; Holt 2005). High-resolution imaging using the *Hubble Space Telescope* (*HST*) with a broad-band red filter (F702W) reveals the source to have a faint, asymmetric halo (de Koff et al. 1996; de Vries et al. 1997). Unlike 3C 459, 3C 213.1 has not been detected in the far-IR by *IRAS* ($L_{\rm IR} < 1.6 \times 10^{11}\,{\rm L}_{\odot}$). Very large array (VLA) images by Akujor & Garrington (1995) at 1.5 and 5 GHz reveal an unusual radio structure for this source that comprises a compact steep spectrum structure of diameter 6 arcsec, and a large diffuse halo that is asymmetric and extends 25 arcsec (69 kpc) south and 10 arcsec (28 kpc) east of the core. At 8.4 GHz, the central structure is resolved into compact components to the north and south which are highly polarized and asymmetrically placed relative to the central core.

It is clear that 3C 213.1 and 3C 459 share many common features. These include intermediate redshifts, disturbed optical morphologies, unusually strong compact steep spectrum radio cores, optical emission lines of relatively low equivalent width, and evidence for YSP components at optical wavelengths. However, despite these similarities, in this paper we demonstrate that the two sources show interesting differences in their stellar populations, and we discuss these differences in the context of evolutionary scenarios for the triggering of the activity. In addition, we discuss the efficacy of different approaches to the modelling of the optical spectra of such sources.

For consistency with other studies of radio source host galaxies and ULIRGs, a Hubble constant of $H_0 = 75\ {\rm km\,s^{-1}\,Mpc^{-1}}$ and a deceleration parameter of $q_0 = 0$ are assumed throughout. For these parameters, 1 arcsec corresponds to 3.18 and 2.90 kpc at the redshifts of 3C 459 and 3C 213.1, respectively.

2 OBSERVATIONS AND REDUCTION

Long-slit spectra for 3C 459 were taken on the night of 2003/09/25 in moderate (1.3 arcsec FWHM) seeing conditions using the FORS2 instrument on the European Southern Observatory Very Large Telescope (ESO VLT). The slit was oriented along PA5 degrees, and the observations comprised 3×900 s exposures with the 600B+22 grism and 3×900 s exposures with the 600RI+19 grism, with the red and blue exposures interleaved to ensure similar atmospheric conditions for observations in the two wavelength ranges. In order to ensure high spectrophotometric accuracy, and avoid problems with differential refraction, the linear atmospheric dispersion compensator was reset between exposures. The data were reduced using the IRAF package, following the usual steps of bias subtraction, wavelength calibration, flux calibration, correction of spatial distortions and spatial registration between the red and blue long-slit spectra. The final useful wavelength range covered by the observations was 3600–8170 Å. The observing conditions were photometric, and observations of several flux calibration standard stars over the two night observing run were used to achieve a relative flux calibration accuracy of better than ±5 per cent. Use of a 1.3 arcsec slit resulted in spectral resolutions of 5 and 6 Å for the blue and red spectral ranges, respectively. Our main analysis for 3C 459 is based on a 1D spectrum extracted from a 1.3×1.5 aperture centred on the continuum nucleus. For comparison, we also examine spectra for 1.3×1.5 arcsec apertures centred 1.75 arcsec (5.5 kpc) to the north and south of the nuclear aperture along PA5. The wider spectral coverage, high spectral resolution, higher signal-to-noise ratio (S/N) and better flux calibration of these data allow us to model the spectra more accurately, and in greater detail, than the study presented in Tadhunter et al. (2002).

The data for 3C 213.1 were taken using the Intermediate dispersion Spectrograph and Imaging System dual beam spectrograph on the 4.2-m William Herschel Telescope (WHT) on the night of 2002/07/14. Use of the R300B and R316R gratings along with a 1.3 arcsec slit resulted in spectral resolutions of 4.13 and 4.58 Å on the red and blue arms, respectively. The observations, comprising 3×1200 s exposures on both arms, cover 3300–6800 Å on the blue arm and 7700–9200 Å on the red arm; they were taken at low airmass in 0.9 arcsec (FWHM) seeing conditions, with the slit aligned along the parallactic angle (PA80). The data reduction steps were the same as those used for 3C 459, and the level of accuracy achieved in both the relative flux and wavelength calibrations was similar. The analysis for 3C 213.1 is based on a single 1.3×3.6 arcsec aperture centred on the nucleus of the galaxy. However,

given the S/N of the data it was not possible to extract spatial information for the stellar populations in this galaxy.

In addition to the spectroscopic data, we also obtained *HST* images for the sources from the *HST* archive. These images – taken with the WFPC2 instrument – were reduced using the standard pipeline processing procedures, with the addition of post-pipeline cosmic ray removal using the IRAF package. For the photometric calibration of these data, we have used the standard photometric calibrations given in the image header files.

3 RESULTS

In Figs 1 and 2, we present the rest-frame optical spectra for 3C 459 and 3C 213.1. These spectra have been corrected for the effects of

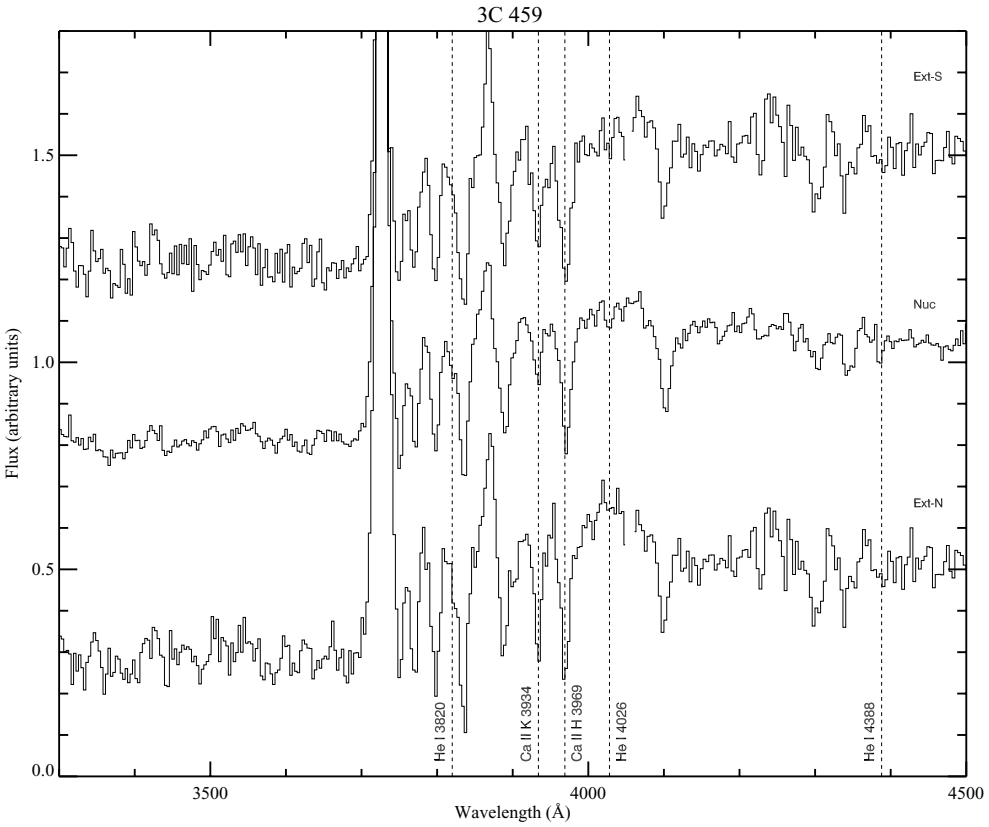

Figure 1. VLT spectra of the three apertures extracted for 3C 459, highlighting the detection of the He I absorption lines in the nuclear aperture (middle spectrum). For clarity, the spectra for the two extended apertures (upper and lower spectra) have been shifted arbitrarily in the vertical direction, but the relative vertical scaling is otherwise the same for all three apertures.

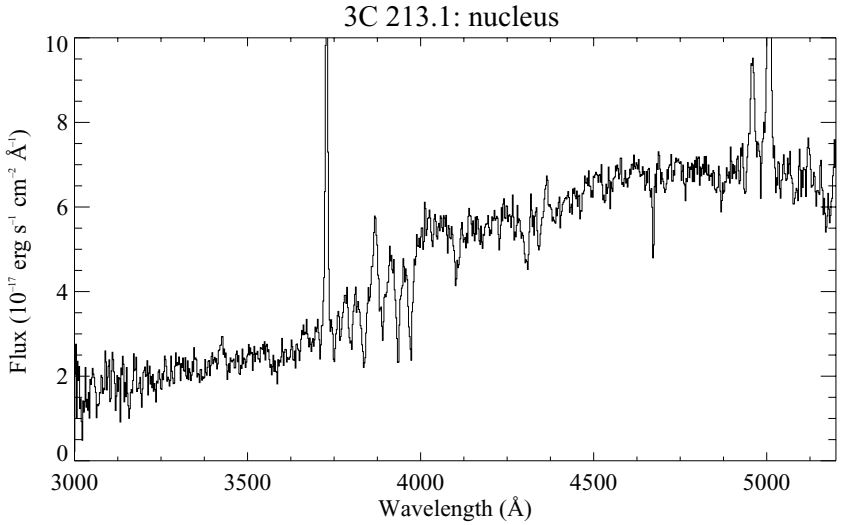

Figure 2. WHT spectrum of the nuclear aperture of 3C 213.1. Only the blue arm spectrum is shown in order to highlight the region around the Balmer break.

Galactic reddening using the Seaton (1979) extinction curve and the values of $E(B-V)$ derived from the full-sky dust map presented in Schlegel, Finkbeiner & Davis (1998). In both cases, we have also subtracted the nebular continuum and higher order Balmer emission lines (H9 and above) following the technique outlined in Dickson et al. (1995) and Holt, Tadhunter & Morganti (2003). Because the Hβ emission line is strongly affected by an underlying stellar photospheric absorption line associated with the YSP present in these galaxies, the Hα emission line was used rather than Hβ to estimate the level of the nebular continuum. Further, we made no attempt to redden the nebular continuum to take into account the possible effects of dust in the host galaxies. Therefore, the estimate based on the Hα line is likely to represent an upper limit on the true level of the nebular continuum in the blue/UV. However, since the overall level of the nebular continuum is low – representing <10 per cent of the UV continuum flux – the failure to take into account reddening in the nebular continuum does not have a major impact on our general results. Indeed, tests in which we model our spectra with either the maximal nebular continuum subtraction based on unreddened Hα or no nebular continuum subtraction produce broadly similar results.

Based on the presence of higher order Balmer absorption lines and a strong Balmer continuum, it is immediately clear from a cursory inspection of the spectra that YSP make a major contribution to the optical/UV continua of both objects. It is also notable that in addition to the detection of the Balmer lines, He I$\lambda\lambda$3819,4026 and maybe He Iλ4388 absorption lines are detected in the nuclear spectrum of 3C 459 (see Figs 1 and 5). These represent the first detections of He I absorption lines in a radio galaxy, providing evidence for a major contribution to the optical emission from post-starburst YSP in the age range $10 < t_{\rm YSP} < 80$ Myr – corresponding to the age of the main-sequence turn-off point of B-type stars (González Delgado et al. 1999). On the other hand, the detection of Ca II K λ3934 and CHλ4314 (*G*-band) features indicates that older stellar populations must also be present in both objects.

The extended apertures in 3C 459 sample regions $\sim$5 kpc north and south of the nucleus along PA5, and it is interesting to compare their spectra with that of the nuclear aperture. The comparison is presented in Fig. 1, which reveals a general similarity between the optical spectra of the nuclear and extended apertures in terms of the overall strength of the Balmer absorption lines and Balmer break.[1] However, one clear difference is that the Ca II K and *G*-band absorption features are relatively stronger in the extended apertures. Given the lack of evidence for substantial reddening of the YSP (see below) or strong Na I$\lambda\lambda$5890,5896 absorption in any of the regions sampled, it is likely that the Ca II K features are formed in the photospheres of stars in the host galaxies, rather than by a screen of absorbing interstellar medium (ISM). Therefore, the variations in both the Ca II K and *G*-band features are likely to reflect genuine gradients in the mix of stellar populations across the galaxy.

In the following sections, we describe the detailed modelling of the spectra.

3.1 Continuum modelling

We used the full blue to red spectral coverage of our extracted spectra to determine the properties of the YSP in both galaxies. Initially, we adopted the approach of modelling the data with the minimum number of components required to give an adequate fit to both the overall SEDs and stellar absorption features, using a purpose-written IDL routine (CONFIT) that fits two stellar components with or without an additional power-law component (Robinson et al. 2000; Robinson 2001). For this initial modelling attempt, we investigated the following two model combinations.

(i) *Young and old.* In this case, we considered combinations of a reddened YSP with ages in the range 0.001 to 5 Gyr plus an unreddened OSP of age 12.5 Gyr. The latter is included because powerful radio sources are generally believed to be hosted by elliptical host galaxies. Note that this is appropriate for a formation redshift for the bulk OSP at $z_{\rm f} \sim 20$ in the adopted cosmology.

(ii) *Young, old and power law.* This combination includes a reddened YSP, unreddened OSP and a power law with spectral index in the range $-15 < \alpha < 15$ ($F_\lambda \propto \lambda^{+\alpha}$). In this case, the power law is included to represent either a very young stellar population (VYSP; $t_{\rm YSP} < 0.01$ Gyr) or an AGN continuum component (e.g. scattered or direct AGN continuum; see Tadhunter et al. 2002). Note, however, that there is no evidence that an AGN continuum makes a major contribution in either object: the emission line equivalent widths are relatively small, we find no signs of broad permitted lines in optical spectra, neither object shows evidence for an unresolved nucleus in optical *HST* images, and, in the case of 3C 459 at least, the UV polarization is low (Tadhunter et al. 2002). Therefore, where present, the power law is likely to represent a VYSP component.

The stellar components were generated using the Bruzual & Charlot (2003) instantaneous burst models with an Salpeter (1955) initial mass function (IMF) and solar metallicity. We considered combinations in which the YSP was reddened using the Seaton (1979) extinction curve with values of $E(B-V)$ in the range 0 to 1.6 mag. The models were then generated by using a normalizing continuum bin of 4720–4820 Å. A series of models was created for every age and reddening for the YSP component combined with an unreddened OSP component (plus power law for the second combination). The models were compared with the fluxes measured from the spectra in several wavelength bins that were chosen to be as uniformly spread in wavelength as possible, and to avoid strong emission lines and atmospheric absorption features. An error of $\pm$5 per cent was assumed for each bin to take into account the estimated uncertainty in the relative flux calibration. A reduced chi-squared test was used to compare each model combination to the data, in addition to a closer visual examination of the model fits in the region of the Balmer break (3500–4500 Å). Based on our previous experience with modelling radio galaxy spectra of similar quality using the same technique, models with $\chi^2_{\rm red} \leqslant 1.0$ were deemed to represent an acceptable fit to the overall continuum shape (see Tadhunter et al. 2005; Holt et al. 2007). Following the SED modelling, detailed examination of the fits to absorption features (e.g. higher order Balmer, He I, Ca II K and *G*-band features) was used to further narrow down the range of viable models.

As well as this 'minimum components' approach, we have also fitted the spectra using the STARLIGHT code (www.starlight.ufsc.br) of Cid Fernandes et al. (2005). This allows a check on the sensitivity of our results to the modelling technique employed, and also provides an interesting comparison between the techniques that are commonly used to model data of this type. In contrast to CONFIT, the STARLIGHT approach consists of fitting the observed spectrum with a combination of several simple stellar populations (SSP) from evolutionary synthesis models. Extinction is modelled by a foreground dust screen, and the version of STARLIGHT we have used assumes that all the stellar components have the same extinction,

[1] Note that the relatively low S/N of the spectra precludes the detection of He I absorption lines in the extended apertures.

Table 1. Best-fitting two- and three-component CONFIT models for 3C 459 (nuclear and extended apertures), and best-fitting two-component model for 3C 213.1 (nuclear aperture). Columns 2–4 give the percentage flux contributions of YSP, OSP and power-law components that give acceptable fits to the SEDs and absorption features, Column 5 gives the best-fitting power-law spectral indices (power-law fits only), while the final four columns give the range of ages, reddenings and masses of the YSP and OSP components corresponding to these fits. Note that, in the case of the power-law fits for 3C 459, the YSP mass will underestimate the total mass in all the YSP components that contribute to the spectrum, because the mass in the very young YSP component represented by the power-law is not taken into account.

Object	Aperture	per cent YSP	per cent OSP	per cent PL	α	Age YSP (Gyr)	$E(B-V)$ YSP (mag)	Mass YSP $\times 10^9 (M_\odot)$	Mass OSP $\times 10^{10}$ ($M_\odot$)
3C 459	Nucleus	62–96	0–40	–	–	0.04–0.07	0.1–0.4	2–9	0 - 10
	Nucleus	42–64	0–16	36–50	−1.6 to −0.4	0.2–0.5	0.0–0.4	3–30	0–5
	ExtN	41–59	0–4	42–56	−1.3 to −0.2	0.5–0.7	0.0–0.3	1–6	0–0.3
	ExtS	64–71	0	29–36	−2.4 to −1.3	0.5–0.6	0.0–0.2	1–3	0
3C 213.1	Nucleus	37–77	24–66	–	–	0.4–0.8	0.0–0.1	2–10	3–7

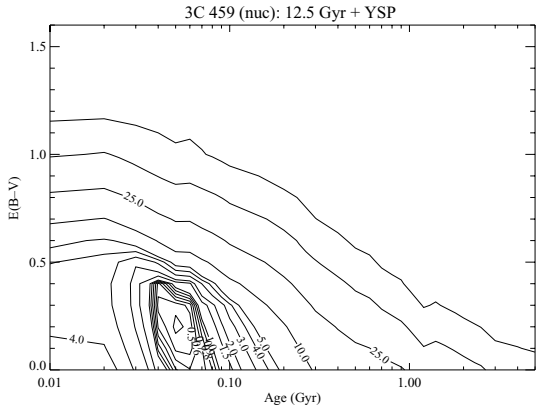

Figure 3. The results of fitting the simple two-component models to the nuclear spectra of 3C 459. The contours show the $\chi^2_{\rm red}$ of the best-fitting models for different combinations of YSP reddening and age.

parametrized as the extinction in the V band (A_V). The output is the population vector that represents the fractional contribution of each SSP (of given age and metallicity) at a wavelength of 4020 Å. The fit is carried out with a simulated annealing plus metropolis scheme, which searches for the minimum chi-square between the observations and the combined models. For the results presented here, we used STARLIGHT with 11 SSPs, corresponding to the ages 4, 5, 10, 25, 40, 100, 280, 500, 890 Myr and 1.3 and 14 Gyr from spectral synthesis models by González Delgado et al. (2005). Note that the latter models employ the Granada synthetic spectral library (www.iaa.es/rosa) built at 0.3 Å spectral resolution (Martin et al. 2005). In contrast, Bruzual & Charlot (2003) models use the empirical STELIB library (webast.ast.obs-mip.fr/stelib) at ∼3 Å spectral resolution (Le Borgne et al. 2003). For the STARLIGHT fits, we use solar metallicity and the Calzetti et al. (2000) extinction law.

3.1.1 3C 459

Initially, we fitted the nuclear spectrum of 3C 459 with the simplest (OPS+YSP) model combination. In this case, we found that the best-fitting models to the overall SED shape consist of a YSP with age in the range $0.04 < t_{\rm YSP} < 0.06$ Gyr and relatively modest reddening [$0.1 < E(B-V) < 0.4$ mag] that dominates the optical spectrum (>75 per cent of flux in the normalizing bin), combined with an OSP that makes a relatively minor (<25 per cent) contribution. The model results are shown in Table 1 and Figs 3 and 4. Detailed examination of the model fits for this combination reveals that they are only partially successful (see Fig. 5). Although the Ca II K, He I lines and G-band features are well fitted, the strengths of the cores of the higher order Balmer lines are significantly overpredicted by this model combination. Note that this apparent overprediction cannot be due to emission line in-filling because the high-order Balmer emission lines were explicitly subtracted prior to the SED fitting as part of the nebular continuum subtraction process, using the maximal nebular continuum derived from the Hα emission line. Moreover, we have experimented with smoothing the models to account for any potential mismatch between the model and data spectral resolution, but find that we cannot significantly improve the fits to the Balmer lines in this way without worsening the fits elsewhere. The masses in the YSP component[2] for these simple model fits are in the range $(2-9) \times 10^9$ $M_\odot$ or 2–100 per cent of the total stellar mass in the regions encompassed by the nuclear aperture.

One possible explanation for the relatively poor fits to the Balmer absorption lines is that VYSP ($t_{\rm YSP} < 0.01$ Gyr) make a significant contribution to the optical spectrum. Such VYSP have relatively featureless spectra with weak Balmer lines and Balmer break, and their presence will act to dilute the Balmer absorption lines in the overall model spectrum. In order to explore this possibility, we also fitted the 3C 459 nuclear spectrum with the second model combination that uses a power law to represent the VYSP component. In this case, we obtained an adequate fit to the Balmer lines, as well as the Ca II K line and the G band, using the combination of a power law and an intermediate-age YSP [$0.2 < t_{\rm YSP} < 0.5$ Gyr, $0.0 < E(B-V) < 0.4$] that contribute roughly equally in the normalizing bin, plus a small (<20 per cent) contribution from an OSP. The corresponding YSP masses fall in the range (3–30) $\times$ 10^9 $M_\odot$ or 5–100 per cent of the total stellar mass in the aperture. The only drawback of this model combination is that it fails to reproduce the strength of the He I lines (see Fig. 5). However, we note that this may be a consequence of modelling the VYSP component with a power law, which is only an approximation to the detailed spectrum of the younger YSP components.

Finally, we have modelled the 3C 459 nuclear spectrum using the STARLIGHT code that allows several stellar components to be fitted simultaneously. Using STARLIGHT, we find that we can obtain excellent fits to all of the stellar absorption lines in the nuclear

[2] The masses for the YSP and OSP were calculated separately using the spectral synthesis model results, which give an effective mass-to-light ratio (M/L) for each stellar component in the normalizing bin. These estimates take full account of any reddening.

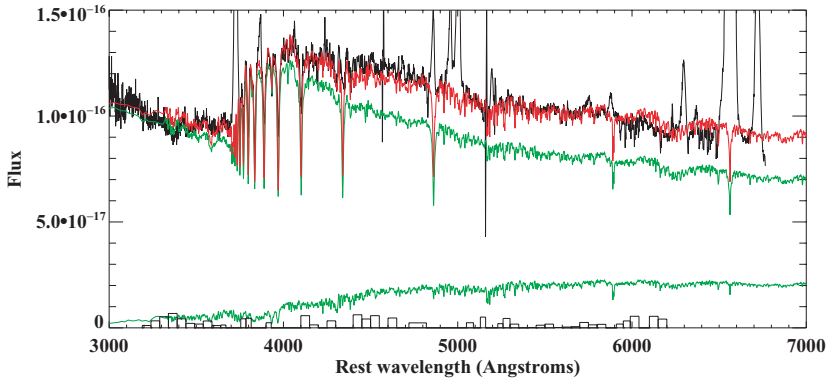

Figure 4. The fit of one of the best-fitting two-component models to the nuclear spectrum of 3C 459, showing the various components of the fit. The plotted model comprises a combination of 12.5 Gyr OSP and 0.04 Gyr YSP, the latter reddened by $E(B-V) = 0.3$. The observed spectrum is shown in black, the best-fitting model in red and the upper green line represents the YSP component, while the lower green line represents the OSP component. The moduli of the differences between the data and the model in the various wavelength bins are shown in histogram form at the bottom of the plot.

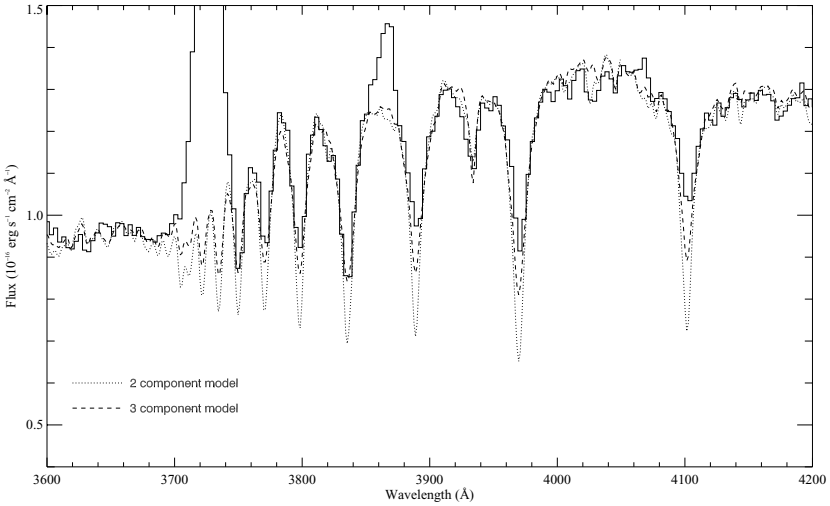

Figure 5. An expanded view of the nuclear spectrum of 3C 459 (solid line) showing the fit of the two-component (OSP+YSP – dotted line) and three-component (OSP+YSP+power law – dashed line) models to the higher order Balmer lines and Ca II K. It is clear that the three-component models provide the best fits to the Balmer line cores, but at the expense of worse fits to the Ca II K and He I lines.

spectrum of 3C 459, including the Balmer and He I lines, as well as to the overall SED. The best-fitting STARLIGHT models comprise the following combination of YSP components with different ages: 0.004–0.005 Gyr (40 per cent),[3] 0.04 Gyr (35 per cent) and 0.5–0.9 Gyr (25 per cent) (all reddened by $A_V = 1.1$). This model is shown in Fig. 6. Note that this particular model does not require any contribution from an OSP to provide an adequate fit to the data. Also, the contribution from the intermediate-age YSP is smaller in these models than in our simple models that include a power law.

Despite the differences between the modelling approaches, and potential issues related to the uniqueness of the *detailed* solutions given the wide range of possible age and reddening combinations, on the basis of the modelling we can make the following robust statements.

(i) The OSP contributes little, if at all, to the nuclear spectrum of 3C 459 – the maximum OSP flux contribution is 20 per cent;

(ii) a combination of younger ($t_{\rm YSP} \leqslant 0.05$ Gyr) and intermediate ($0.1 < t_{\rm YSP} < 1.3$ Gyr) age YSP components is essential to fit the data.

(iii) A VYSP ($t_{\rm YSP} < 0.01$ Gyr) component is also required in order to fit the higher order Balmer lines adequately.

(iv) The relative importance of the intermediate-age YSP in the solutions depends on the way the younger YSP components are handled in the models, and on whether an OSP component is included.

(v) The line-of-sight reddening to the YSP components is relatively modest in all successful models [$E(B-V) < 0.4$].

We have also modelled the spectra of the extended apertures in a similar manner. We find that we are unable to model the overall SEDs, Balmer lines, Ca II K and *G* band of the extended apertures adequately using the simplest two-component models (OSP+YSP). For example, fits using YSPs with similar ages to those required for the two-component fits to the nuclear aperture data ($t_{\rm YSP} \sim 0.04$–0.05 Gyr) substantially underpredict the strengths of the Ca II K and *G*-band features, and provide a generally poor fit to the continuum shape in the region of the Balmer break. In contrast, adequate fits to

[3] These are the percentage flux contributions of the stellar components at 4020 Å.

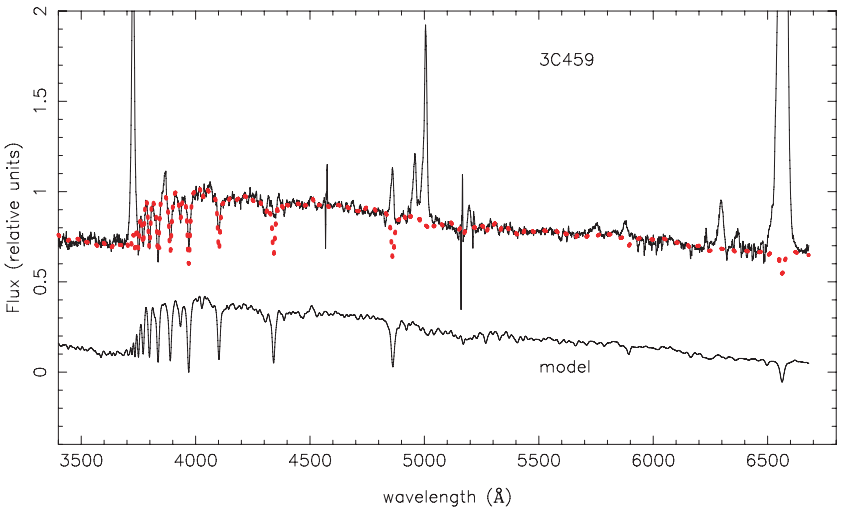

Figure 6. STARLIGHT fit to the nuclear spectrum of 3C 459. The dotted line shows the fit to the data (upper solid line), while the lower solid line is the model spectrum shifted for ease of comparison.

all absorption features and the overall SED shape can be obtained using a combination of intermediate-age YSP and power-law (VYSP) components. The latter models do not require an OSP component. Note also that, although the proportional contribution of the YSP for the extended apertures is similar to that in the nuclear aperture, the age range of the viable fits for the extended apertures ($0.5 < t_{\rm YSP} < 0.7$ Gyr) is older on average than for the nucleus – consistent with the stronger Ca II K and *G*-band absorption in those apertures. The results for the YSP plus power-law fits to the spectra of the extended apertures are presented in Table 1.

3.1.2 3C 213.1

In the case of the nuclear spectrum of 3C 213.1, we find that we can obtain good fits to the overall SED using a simple combination of an intermediate-age, moderately reddened YSP [$0.2 < t_{\rm YSP} < 1.5$ Gyr, $0.1 < E(B-V) < 0.5$ mag] and an OSP. An example of one of the best-fitting two-component models is shown in Fig. 7, while the minimum χ^2 results obtained for various combinations of YSP age and reddening are presented in Fig. 8 as a contour plot. However, adequate detailed fits to the stellar absorption lines are

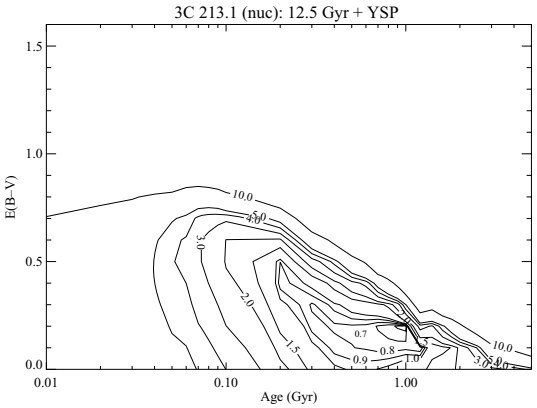

Figure 8. The results of fitting the simple two-component models to the nuclear spectra of 3C 213.1. The contours show the $\chi^2_{\rm red}$ of the best-fitting models for different combinations of YSP reddening and age.

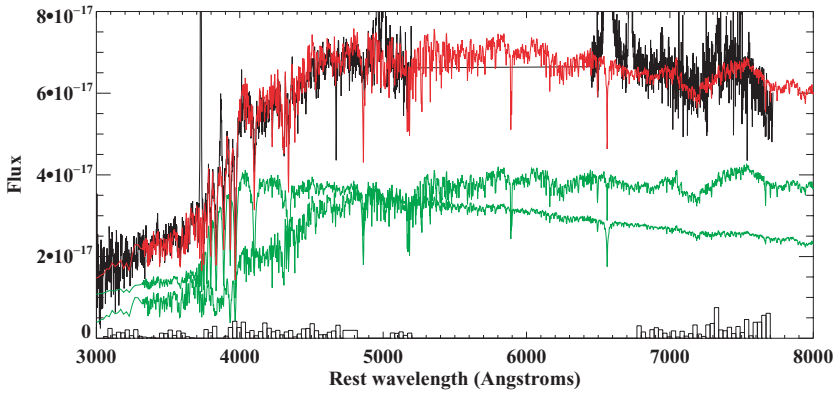

Figure 7. The fit of one of the best-fitting two-component models to the nuclear spectrum of 3C 213.1, showing the various components of the fit. The plotted model comprises a combination of 12.5 Gyr OSP and unreddened 0.3 Gyr YSP. The observed spectrum is shown in black, the best-fitting model in red, while the two green lines represent the YSP and OSP components. The moduli of the differences between the data and the model in the various wavelength bins are shown in histogram form at the bottom of the plot.

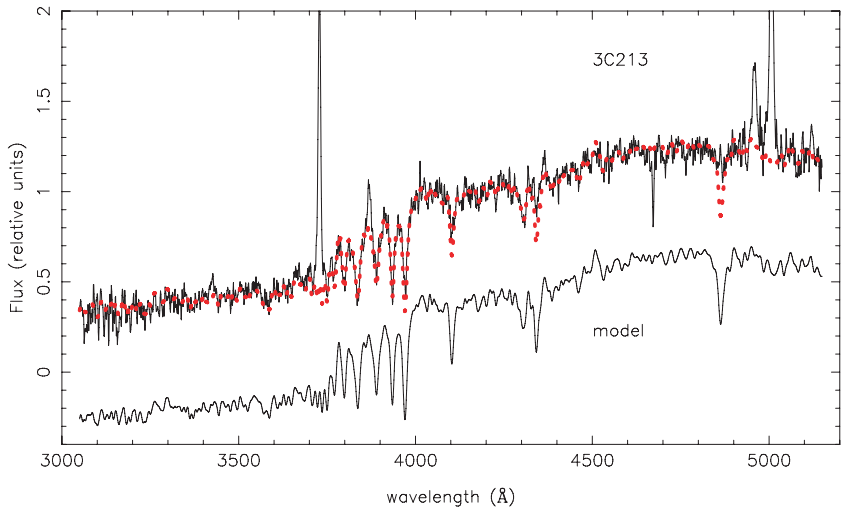

Figure 9. STARLIGHT fit to the nuclear spectrum of 3C 213.1. The dotted line shows the fit to the data (upper solid line), while the lower solid line is the model spectrum shifted for ease of comparison.

only obtained for YSP ages in the range $0.4 < t_{\rm YSP} < 0.8$ Gyr – the Ca II K line is under- or over-predicted for younger or older YSP ages, respectively. The overall best-fitting model parameters are presented in Table 1. In this case, the total mass in the YSP component is in the range $(2 - 10) \times 10^9\,{\rm M}_\odot$, or 3–33 per cent of the total stellar mass in the region sampled by the nuclear aperture.

Given the large wavelength gap between the blue and red spectra, which prevents us from checking the accuracy of the relative flux calibration by comparing the flux levels in an overlap region, we have also modelled the blue spectrum by itself. The results obtained from model fits to the blue spectrum are entirely consistent with those obtained by modelling the blue and red spectra together.

In contrast to the situation for 3C 459, we find that the addition of a power-law component does not significantly improve the fits. Moreover, attempts to model the spectrum using the multicomponent STARLIGHT code provide no evidence for a younger YSP component (<0.1 Gyr). Indeed, the STARLIGHT results suggest that the nuclear spectrum can be adequately fitted without significant contributions from either a younger YSP component ($t_{\rm YSP} < 0.1$ Gyr) or an OSP component, with the best results obtained for the following contributions of intermediate-age YSP components: 0.1 Gyr (14 per cent), 0.9 Gyr (30 per cent), 1.3 Gyr (59 per cent) (all reddened by $A_V = 0.95$ mag). The latter model fit is illustrated in Fig. 9.

It is clear that, while the nuclear spectrum of 3C 459 is dominated by younger YSP components ($t_{\rm YSP} < 0.05$ Gyr), with a relatively minor contribution from intermediate-age YSP, the younger YSP components are entirely absent in 3C 213.1. The exact ages of the intermediate-age YSP that are required to model the nuclear spectrum of 3C 213.1 depend on the number of components included in the model, and also on whether an OSP component is included.

3.2 The photometric properties of the host galaxies

In terms of gauging their evolutionary status, it is also interesting to consider the morphologies and photometric properties of the host galaxies of 3C 213.1 and 3C 459.

The relatively shallow but high-resolution F702W image of 3C 459 shown in Fig. 10 reveals that it has a dominant high surface brightness core surrounded by an elliptical-like envelope. However, this object is clearly not an undisturbed elliptical galaxy because

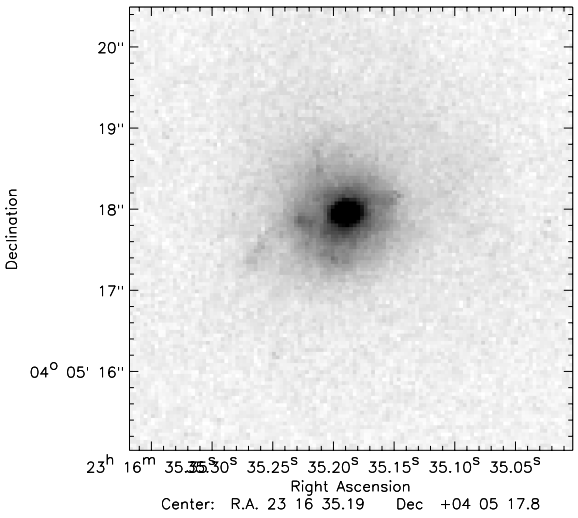

Figure 10. Broad-band image of *HST* image of 3C 459 taken using the WFPC2 camera with an F702W filter. North is to the top and east to the left.

the *HST* image also reveals a complex sub-structure that consists of a series of compact knots extending to a radius of ∼4 kpc to the north and east of the nucleus. On a larger scale, deep ground-based images also show a fan-like structure extending ∼24 kpc to the east of the nucleus (Heckman et al. 1986). In a quantitative analysis of *HST* images of ULIRGs by Conselice (2003), 3C 459 has the highest concentration index of all the ULIRG systems included in the study – consistent with the original morphological classification of this object as an N-galaxy – and has a larger asymmetry index than expected for an undisturbed elliptical galaxy. All of these features are consistent with the idea that 3C 459 has been involved in a major merger in the recent past.

In terms of photometric properties, we have used the F702W image of 3C 459 to determine its absolute luminosity in a 10 arcsec (32 kpc) diameter aperture centred on the nucleus. The details are shown in Table 2. Note that, although the derived absolute *R*-band luminosity ($M_R = -22.22$) within the 10 arcsec aperture is close to the average measured for radio and quasar host galaxies at similar redshifts (Dunlop et al. 2003), this does not provide a true indication

Table 2. Photometric properties of 3C 459 and 3C 213.1. Columns 2–4 give the F702W *HST*/WFPC2 magnitudes for the two objects measured in a 10 arcsec circular aperture, the equivalent Cousins *R*-band magnitude and the Cousins R absolute magnitude; Column 5 gives the *R*-band absolute magnitude corrected for the YSP contribution estimated from the modelling of our spectra, and Column 6 gives the estimates of the *R*-band total magnitude corrected for apertures and YSP. In making these calculations, we have assumed $m_{702} - m_R = -0.2$, and an *R*-band *K*-correction of $K_R = 0.2$ appropriate to the spectral types and redshifts of the objects (Fukugita, Shimasaku & Ichikawa 1995).

	10 arcsec aperture			Cor.	Total
Object	m_{702}	m_R	m_R	m_R	m_R
3C 459	17.75	17.95	−22.22	−20.5	−21.6
3C 213.1	18.19	18.39	−21.43	−21.0	–

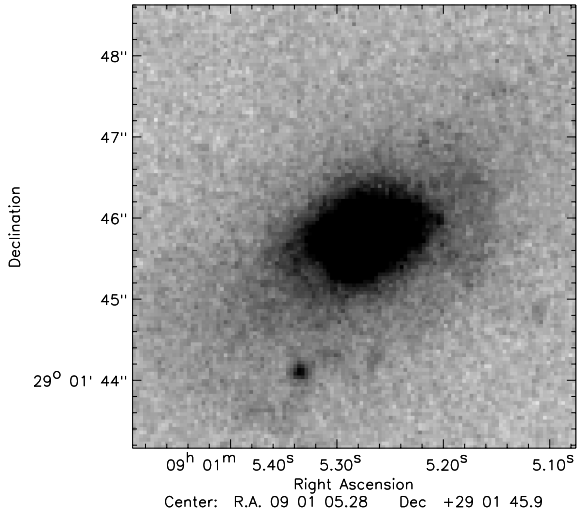

Figure 11. Broad-band image of *HST* image of 3C 213.1 taken using the WFPC2 camera with the F702W filter.

of the luminosity of the old stellar bulge component in the galaxy. On the basis of our spectroscopic analysis, we find that the *maximum* contribution of OSP in the relevant bands is 20 per cent. Moreover, photometric results based on deep *K*-band imaging observations (Inskip et al., in preparation) suggest that the contribution of light from the halo of the galaxy outside the 10 arcsec aperture would boost the flux of the OSP by at most a factor of ×2.82. Taking all of these factors into account, and assuming that the mix of stellar populations remains constant across the 10 arcsec photometric aperture, our best estimate of the total absolute *R*-band luminosity of the old stellar component of 3C 459 is $M_R = -21.7$. This places 3C 459 at the lower end of the range of absolute luminosities for quasar and radio galaxy hosts (Dunlop et al. 2003), and corresponds to $\sim 1.5L_*$ (adopting $M_R^* = -21.3$ from Lin et al. 1996[4]).

We have less information about the morphological and photometric properties of 3C 213.1. The F702W *HST* image shown in Fig. 11 reveals that this galaxy is less centrally concentrated than 3C 459, and that there is less evidence for knotty sub-structure in the envelope of the galaxy. However, the outer envelope is clearly asymmetric, suggesting a high degree of tidal disturbance in the recent history of the system. 3C 213.1 is also fainter than 3C 459: the 10 arcsec (29 kpc) aperture absolute magnitude of the source ($M_R = -21.43$) is less luminous than any of the radio galaxy and quasar hosts in the sample of Dunlop et al. (2003). On the basis of our spectroscopic analysis, a maximum of 70 per cent of the *R*-band light in the nuclear aperture is contributed by an OSP. Assuming that this result holds across the entire 10 arcsec photometric aperture, the maximum luminosity of the OSP in this aperture corresponds to $M_R = -21.0$. Unfortunately, we lack accurate photometric information for the region outside the 10 arcsec aperture for this source, but even allowing for an aperture correction of similar level to that found for 3C 459, it is clear that the luminosity of the OSP component in the bulge of 3C 213.1 cannot be much above $2L_*$.

Overall, we deduce that the luminosities of the old stellar bulges in both sources are at the lower end of the range measured for radio galaxy and quasar hosts at similar redshifts. These results demonstrate the importance of taking into account the YSP components when investigating the properties of the bulges of the host galaxies, with implications for the determination of black hole masses using the correlation between the absolute luminosities of the stellar bulges and the black holes masses.

4 DISCUSSION

4.1 Triggering and evolution

The disturbed optical morphologies and the presence of massive YSP components in the host galaxies of the two radio sources investigated in this paper support the idea that the AGN have been triggered in gas-rich mergers which have also triggered major episodes of star formation. However, 3C 459 and 3C 213.1 represent contrasting cases in terms of the detailed properties of their YSP components.

The optical spectrum of 3C 459 is dominated by younger YSP components ($t_{\rm YSP} < 0.05$ Gyr), but with a significant contribution from intermediate-age YSP components. Such YSP properties – especially the dominance of the younger YSP components – appear typical of ULIRGs as a class (Canalizo & Stockton 2001; Rodríguez-Zaurín et al., in preparation). In terms of the evolutionary models, the presence of both young and intermediate-age YSPs in 3C 459 is consistent with simulations of star formation in major gas-rich mergers. In particular, the younger YSP components, as well as the ULIRG activity, are likely to represent the starburst induced by the tidal forces as the nuclei of the two galaxies coalesce in the final stages of the merger. The simulations predict that this phase will last of the order of ∼0.1 Gyr (Mihos & Hernquist 1996; di Matteo et al. 2005) – in line with the YSP ages we estimate for the younger YSP components in 3C 459. The fact that the system has a single, rather than double, nucleus is also consistent with the idea that we are observing it shortly after the coalescence of the two nuclei. On the other hand, the properties of the intermediate-age YSP component are consistent with a first burst of star formation that is predicted to occur around the first pass of the two merging galaxies, some 0.5–1.0 Gyr before the two nuclei merge together (Mihos & Hernquist 1996). Given that the lifetimes of extragalactic radio sources are generally assumed to be $t_{\rm jet} \leqslant 0.1$ Gyr, our results are consistent with the idea that the radio jet and AGN activity have been triggered close to the peak of star formation activity as the merging nuclei coalesce.

In contrast, 3C 213.1 presents no evidence for the younger YSP components, although, like 3C 459, it has a massive

[4] This L_* absolute magnitude has been converted to our cosmology, and we have used the same factor for correction of aperture to total magnitude as Dunlop et al. (2003).

intermediate-age YSP component. It is also notable that 3C 213.1 lacks the luminous far-IR emission detected in the case of 3C 459. This lack of evidence for recent or ongoing star formation suggests that we are not observing 3C 213.1 at a time close to the coalescence of the nuclei in a major gas-rich merger. However, this does not rule out the possibility that the system has undergone a major gas-rich merger *in the past*. In fact, the properties of the intermediate-age YSP are consistent with a major starburst ∼0.4–1.4 Gyr ago that might plausibly have been triggered by a gas-rich merger. In addition, assuming that the radio source in this object is not unusually long-lived, there must have been a significant time lag ($\geqslant$0.3 Gyr) between the coalescence of the nuclei in the merger and triggering of the current phase of jet/AGN activity. This is similar to the cases of 3C 293, 3C 305 and B2 0648+27 presented in Tadhunter et al. (2005) and Emonts et al. (2006). As discussed in the former paper, a time lag could occur for a number of reasons, including the time-scale required for black holes in the merging nuclei to finally coalesce and form a spinning supermassive black hole, and the time-scale for the gas to lose sufficient angular momentum to be accreted close to the black hole and fuel the activity.

It is possible, however, that the idea of a single AGN triggering event is oversimplistic, and that the AGN is triggered more than once in the course of a merger. It is important to recognize that galaxy mergers are complex events, and the merger debris will continue to rain down on the nuclear regions of the remnant for time-scales $\geqslant$0.5 Gyr, leading to one or more AGN re-triggering events as fresh supplies of gas are accreted on to the nuclear regions. Therefore, despite the differences between the detailed properties of their YSP, it is plausible that 3C 459 and 3C 213.1 represent different stages in the same evolutionary scenario, with 3C 459 triggered close to the peak of the star formation in the merger as the two nuclei coalesce, and 3C 213.1 representing a late time re-triggering of the activity some hundreds of Myr after the main merger-induced starburst. It is notable that the complex radio structure of 3C 213.1, with an inner compact double structure aligned with a more extended outer envelope (Akujor & Garrington 1995), is consistent with this object having undergone more than one phase of activity.

4.2 Modelling the stellar populations in radio galaxies

The quality of the data, and dominance of the YSP components for the two objects considered in this paper, allows us to make an interesting comparison between the various modelling approaches.

The simplest CONFIT two-component (OSP+reddened YSP) modelling approach – the approach used for most other radio galaxies that have lower quality data and/or less dominant YSP components – provides a useful indication of the luminosity-weighted age of the reddened YSP component. This approach appears entirely adequate for 3C 213.1, which is dominated by an intermediate-age YSP, but fails to reproduce the details of the absorption line spectrum in the case of 3C 459, particularly the high-order Balmer lines. Including a power law to represent a VYSP component in 3C 459 improves the fit to the Balmer lines, but at the expense of a worse fit to the He I lines.

It is clear that, in order to fit the detailed spectrum of 3C 459 adequately, we require a model that combines two or more younger YSP components with an intermediate-age YSP or OSP component. This is where the STARLIGHT code, which allows several YSP components of varying age to be fitted, is particularly useful. Indeed, the results of the STARLIGHT modelling provide an excellent fit to both the detailed absorption line spectrum and the overall SED shape of 3C 459. Given the large number of stellar components included, the main question concerning the STARLIGHT results is one of uniqueness. All spectroscopic data sets will suffer from systematic uncertainties in the flux calibration at some level, and that the version of the STARLIGHT code we have used does not have complete flexibility in allowing different YSP components different degrees of reddening. In this situation, the best mathematical solution in terms of minimizing the residuals between the data and the models does not necessarily reflect the true reality of the stellar populations. Thus, while the results of STARLIGHT are likely to be accurate in the broad-brush sense of indicating the relative contributions of younger YSP, intermediate YSP and OSP components, the degree to which the *details* of the solutions are accurate is unclear (see discussion in Cid Fernandes et al. 2005). For example, we find that we can adequately model the optical/UV spectrum of 3C 213.1 using CONFIT with a two-component (intermediate-age YSP+OSP) model, but the best-fitting STARLIGHT model for this object has contributions from three intermediate-age YSPs of different age. The models agree concerning the dominance of the intermediate-age YSP(s) and the absence of younger YSP components in this case, but uncertainties remain about the weight that should be given to the details of the combination of intermediate-age YSPs required by STARLIGHT. On the other hand, while the CONFIT approach has the advantage of simplicity, its results depend on the stellar components assumed in the fits. In particular, the properties of intermediate-age YSP component required in the best-fitting CONFIT two-component models for 3C 213.1 are dependent on our assumption of a 12.5 Gyr OSP. Clearly, at a detailed level, the results of the spectral synthesis modelling depend on the assumptions made in the different modelling approaches, as well as the stellar evolution models and stellar libraries employed.

5 CONCLUSIONS

The results of this paper reinforce the idea that the radio jet and AGN activity are triggered by major galaxy mergers in at least a subset of the powerful radio galaxy population. However, while there is good evidence that 3C 459 has been triggered at close to the peak of the star formation activity, following the coalescence of the nuclei of the merging galaxies, it is likely that 3C 213.1 has been triggered (or re-triggered) at a later post-merger phase; despite the differences in their YSP properties, these two objects may represent different stages in the same overall process. Thus, the relationship between mergers and the AGN they trigger is not simple, perhaps reflecting the complex reality of gas accretion on to the nuclear regions of the merging galaxies over the full ($>$1 Gyr) lifetime of a typical merger.

Our results also demonstrate that considerable caution is required when deducing the properties of the old stellar bulges of the host galaxies, and hence of the supermassive black holes, based on broad-band photometry alone. It has long been known that activity-related continuum components can significantly contaminate the optical/UV emission of the host galaxies. However, our results show that, even when the host galaxy continuum emission is dominated by starlight, the presence of significant YSP components can lead to the luminosities of the old stellar bulges being substantially overestimated.

ACKNOWLEDGMENTS

KAW thanks the Royal Society for a Dorothy Hodgkin Royal Society Fellowship. JH, KJI and JRZ acknowledge support from PPARC. CT and RDG thank CSIC and the Royal Society for supporting this research through the travel grant 2006GB0070. We thank Roberto

Cid Fernandes for making his STARLIGHT software publicly available, and the anonymous referee for useful comments. The WHT is operated on the island of La Palma by the Isaac Newton Group in the Spanish Observatorio del Roque de los Muchachos of the Instituto de Astrofisica de Canarias. Based in part on observations with the NASA/ESA *HST*, which is operated by the Association for Research in Astronomy (AURA), Inc., under NASA contract NAS5-26555, and on observations collected at the European Southern Observatory telescopes at the Paranal Observatory under programme 71.B-0616(A).

REFERENCES

Akujor C. E., Garrington S. T., 1995, A&AS, 112, 235
Aretxaga I., Terlevich E., Terlevich R. J., Cotter G., Díaz A., Hunstead R., 2001, MNRAS, 325, 636
Bruzual G., Charlot S., 2003, MNRAS, 344, 1000
Calzetti D., Armus L., Bohlin R. C., Kinney A. L., Koornneef J., Storchi-Bergmann T., 2000, ApJ, 533, 682
Canalizo G., Stockton A., 2001, ApJ, 555, 719
Cid Fernandes R., Mateus A., Sodré L., Stasińska G., Gomes J. M., 2005, MNRAS, 358, 363
Conselice C. J., 2003, ApJS, 147, 1
de Koff S., Baum S. A., Sparks W. B., Biretta J., Golombek D., Macchetto F., McCarthy P., Miley G. K., 1996, ApJS, 107, 621
de Vries W. H. et al., 1997, ApJS, 110, 191
Dickson R., Tadhunter C., Shaw M., Clark N., Morganti R., 1995, MNRAS, 273, L29
di Matteo T., Springel V., Hernquist L., 2005, Nat, 433, 604
Dunlop J. S., McClure R. J., Kukula M. J., Baum S. A., O'Dea C. P., Hughes D. H., 2003, MNRAS, 340, 1095
Emonts B. H. C., Morganti R., Tadhunter C. N., Holt J., Oosterloo T. A., van der Hulst J. M., Wills K. A., 2006, A&A, 454, 125
Eracleous M., Halpern J. P., 1994, MNRAS, 90, 1
Fukugita M., Shimasaku K., Ichikawa T., 1995, PASP, 107, 945
Gelderman R., Whittle M., 1994, ApJS, 91, 491
González Delgado R. M., Leitherer C., Heckman T. M., 1999, ApJS, 125, 489
González Delgado R. M., Cervino M., Martins L. P., Leitherer C., Hauschildt P. H., 2005, MNRAS, 357, 945
Heckman T. M., Smith E. P., Baum S. A., van Breugel W. J. M., Miley G. K., Illingworth G. D., Bothun G. D., Balick G. D., 1986, ApJ, 311, 5261
Heckman T. M., O'Dea C. P., Baum S. A., Laurikainen E., 1994, MNRAS, 428, 65
Kauffmann G., Haehnelt M., 2000, MNRAS, 311, 576
Holt J., 2005, PhD thesis, Univ. Sheffield
Holt J., Tadhunter C. N., Morganti R., 2003, MNRAS, 342, 995
Holt J., Tadhunter C. N., González Delgado R. M., Inskip K. J., Rodriguez J., Emonts B. H. C., Morganti R., Wills K. A., 2007, MNRAS, 381, 611
Le Borgne J.-F. et al., 2003, A&A, 402, 433
Lin H., Kirshner R. P., Shectman S. A., Landy S. D., Oemler A., Tucker D. L., Schechter P. L., 1996, ApJ, 464, 60
Martins L. P., González Delgado R. M., Leitherer C., Cerviño M., Hauschild P., 2005, MNRAS, 358, 49
McLure R. J., Kukula M. J., Dunlop J. S., Baum S. A., O'Dea C. P., Hughes D. H., 1999, MNRAS, 308, 377
Mihos C. J., Hernquist L., 1996, ApJ, 464, 641
Miller J. S., 1981, PASP, 93, 681
Raimann D., Storchi-Berbmann T., Quintana H., Hunstead R., Wisotzki L., 2005, MNRAS, 364, 1239
Robinson T. G., 2001, PhD thesis, Univ. Sheffield
Robinson T. G., Tadhunter C. N., Axon D. J., Robinson A., 2000, MNRAS, 317, 922
Salpeter E. E., 1955, ApJ, 121, 161
Sanders D. B., Mirabel I. F., 1996, ARA&A, 34, 749
Schlegel D. J., Finkbeiner D. P., Davis M., 1998, ApJ, 500, 525
Seaton M. J., 1979, MNRAS, 187, 73P
Smith H. E., Spinrad H., 1980, PASP, 92, 553
Spinrad H., Djorgovski S., Marr J., Aguilar L., 1985, PASP, 97, 932
Tadhunter C. N., Morganti R., di Serego Alighieri S., Fosbury R. A. E., Danziger I. J., 1993, MNRAS, 263, 999
Tadhunter C., Dickson R., Morganti R., Robinson T. G., Wills K., Villar-Martin M., Hughes M., 2002, MNRAS, 330, 977
Tadhunter C., Robinson T. G., González Delgádo R. M., Wills K., Morganti R., 2005, MNRAS, 356, 480
Tadhunter C. et al., 2007, ApJ, 661, L13
Thomasson P., Saikia D. J., Muxlow T. W. B., 2003, MNRAS, 341, 91
Wills K. A., Tadhunter C. N., Robinson T. G., Morganti R., 2002, MNRAS, 333, 211
Wills K. A., Morganti R., Tadhunter C. N., Robinson T. G., Villar-Martin M., 2004, MNRAS, 347, 771
Wyndham J. D., 1966, ApJ, 144, 459

This paper has been typeset from a TEX/LATEX file prepared by the author.